Showcasing research from the Osthoff laboratory, Department of Chemistry, University of Calgary, Alberta, Canada.

Thermal decomposition of peroxyacrylic nitric anhydride (APAN)

Graduate student Amanda and undergraduate students Kevin and Nicole studied the thermal decay kinetics of APAN (CH_2═$CHC(O)O_2NO_2$) in lab experiments. While drafting the manuscript, the group deployed to the field to quantify nitrogen oxides in Calgary Inglewood. By chance, the air quality rapidly deteriorated to "among the worst in the world" due to upwind wildfires, obscuring the sky (photo). High APAN concentrations arrived with the acrid air, allowing evaluation of the lab results under real-world conditions while catching a glimpse of a future in which climate change driven wildfires dominate air pollution.

Dwayne Reilander, CC BY-SA 4.0, via Wikimedia Commons.

As featured in:

See Hans D. Osthoff *et al., Environ. Sci.: Atmos.*, 2025, **5**, 801.

ROYAL SOCIETY OF CHEMISTRY

rsc.li/esatmospheres

Registered charity number: 207890

Environmental Science: Atmospheres

ROYAL SOCIETY OF CHEMISTRY

PAPER

View Article Online
View Journal | View Issue

Cite this: *Environ. Sci.: Atmos.*, 2025, **5**, 801

Thermal decomposition of peroxyacrylic nitric anhydride (APAN)†

Amanda L. Gomez, Kevin D. Easterbrook, Nicole M. Johnson, Shanu Johnson and Hans D. Osthoff *

The peroxycarboxylic nitric anhydrides (PANs; $RC(O)O_2NO_2$ with R ≠ H) are important trace gas constituents of the troposphere. One of the lesser studied molecules of the PAN family is peroxyacrylic nitric anhydride (APAN; $CH_2{=}CHC(O)O_2NO_2$) which is found in elevated concentration in biomass burning (BB) plumes and downwind from petrochemical plants. In this work, we conducted laboratory and field experiments to constrain the thermal decomposition (TD) rates of APAN in the atmosphere. The TD of APAN was studied in laboratory experiments using a Pyrex reaction coil at temperatures between 295.2 K and 320.7 K as a function of flow rate (*i.e.*, residence time). Gas streams containing APAN were generated from a diffusion source containing a synthetic sample stored in tridecane at water-ice temperature. Nitric oxide (NO) was added to this gas stream to prevent recombination of the TD products. Concentrations of APAN were monitored by gas chromatography with electron capture detection (PAN-GC). The TD rate constant is best described by $10^{(17.88\pm0.80)}\,e^{-(121.2\pm4.8)\ \mathrm{kJ\ mol^{-1}}/(RT)}\ s^{-1}$, where R is the universal gas constant, and T is the temperature in kelvin. We report ambient air mixing ratios of peroxyacetic nitric anhydride (PAN), peroxypropionic nitric anhydride (PPN), and APAN measured by PAN-GC at the Calgary Central (Inglewood) air quality station from April 17 to May 31, 2023. From May 16 to May 21, the measurement location was blanketed by a BB plume as judged from co-located observations of fine particulate matter ($PM_{2.5}$) and carbon monoxide (CO). During this time, mixing ratios as high as 3.4 ppbv (PAN), 455 pptv (PPN), and 220 pptv (APAN) were observed. After sunset, mixing ratios of the PANs decreased with pseudo-first order kinetics, rationalized by a combination of dry deposition and loss by TD.

Received 1st March 2025
Accepted 30th April 2025

DOI: 10.1039/d5ea00032g

rsc.li/esatmospheres

Environmental significance

The peroxyacyl nitrates (PANs) are important tropospheric trace gases acting as NO_x reservoir species that are removed mainly by thermal decomposition (TD). Peroxyacrylic nitric anhydride (APAN; also called peroxyacryloyl nitrate or vinyl-PAN, $CH_2{=}CHC(O)O_2NO_2$) is found in elevated concentration in motor vehicle exhaust, petrochemical, and biomass burning (BB) plumes. Grosjean *et al.* (1994) studied the TD of APAN but reported Arrhenius parameters at odds with other PAN-type compounds. Here, we report rate constants for APAN's TD measured in laboratory experiments and revised Arrhenius parameters which will allow for more accurate modeling of nitrogen oxides in BB plumes. We also report ambient air measurements of PANs (including APAN) during a BB episode in Calgary and investigated the removal of PANs after sunset.

1. Introduction

Peroxycarboxylic nitric anhydrides (PANs; $RC(O)O_2NO_2$, R ≠ H), also referred to as peroxyacyl nitrates, are important trace gas constituents of the troposphere.[1,2] The simplest and usually most abundant of the PANs is peroxyacetic nitric anhydride (PAN, R = $-CH_3$), commonly referred to as peroxyacetyl nitrate. Its mixing ratio ranges from several parts per billion (10^{-9}, ppbv) in polluted areas to a few parts per trillion (10^{-12}, pptv) in remote regions.[3] Although more than 45 different PANs are known,[2] only a few have been quantified in ambient air. These include peroxypropionic (PPN, R = $-C_2H_5$), peroxyisobutyric (PiBN, R = $-(CH_3)_2CH$), peroxymethacrylic (MPAN, R = $-CH_2{=}C(CH_3)$), and peroxyacrylic nitric anhydride (APAN, R = $-CH_2{=}CH$).[4–7] Observations of APAN (on which this paper focuses) in ambient air have been relatively sparse (Table 1).

The PANs are primarily formed as by-products of photochemical ozone (O_3) and smog production, *i.e.*, from the photooxidation of volatile organic compounds (VOCs) in the presence of NO_x (= NO + NO_2), and are often associated with biomass burning (BB) plumes.[7,12] Aldehydes are usually the most common VOC precursors of PANs. For example, PAN is

Department of Chemistry, University of Calgary, 2500 University Drive N.W., Calgary, T2N 1N4, Alberta, Canada. E-mail: hosthoff@ucalgary.ca

† Electronic supplementary information (ESI) available. See DOI: https://doi.org/10.1039/d5ea00032g

Table 1 Ambient air observations of APAN reported in the open literature. Abbreviations: n/d = not determined; O&G = oil and gas; BB = biomass burning

Reference	Campaign	Platform	Major source type	Max. APAN (pptv)	APAN:PAN (%)
8	RISOTTO 1999–2000	Ground	n/d	65	4
9	TexAQS 2000	Ground	O&G	502	30
10	SENEX 2013	Aircraft	BB	26	5.3 ± 0.7
6	OPECE 2018	Ground	O&G	>400	1–4
7	SUNVEx 2021	Ground	BB	80	3.7 ± 0.1
11	KORUS-AQ 2016	Aircraft	O&G	850	14.2
This work	FOOBAR 2023	Ground	BB	220	4–8

mainly derived from the hydroxyl radical (OH) initiated oxidation of acetaldehyde, and the unsaturated APAN and MPAN are primarily derived from oxidation of acrolein and methacrolein, respectively, *e.g.*,

$$CH_2{=}CHC(O)H + OH \xrightarrow{O_2} CH_2{=}CHC(O)O_2 + H_2O,\ k_1 \quad (R1)$$

Subsequent reaction of the acrolein peroxyacyl (APA) radical with NO_2 yields APAN:

$$CH_2{=}CHC(O)O_2 + NO_2 \rightarrow CH_2{=}CHC(O)O_2NO_2,\ k_2 \quad (R2)$$

Acrolein stems mainly from the photooxidation of 1,3-butadiene, though also has primary sources such as automobile exhaust;[13] acrolein and 1,3-butadiene have also been associated with emissions from petrochemical industries.[11] In contrast, methacrolein is mainly derived from isoprene, which is predominantly biogenic in origin. Consequently, the relative abundances of MPAN and APAN provide insight into whether anthropogenic or biogenic hydrocarbons dominated the O_3 production upwind.[4]

The PANs are important molecules for two main reasons: for one, because their production consumes and their decomposition releases nitrogen dioxide (NO_2), the PANs can act as reservoir species of NO_x and odd oxygen ($O_x = O_3 + NO_2$) and can transport NO_x and O_x from polluted urban air to remote regions where nitrogen oxides are scarce. In this way, the PANs contribute to the redistribution of NO_x and, by extension, affect the rates of tropospheric O_3 and secondary organic aerosol (SOA) production throughout the troposphere.[14,15] The second reason why PANs are important molecules is that the PANs are noxious in high concentration. For instance, PAN has been shown to be phytotoxic,[16] and PAN and PPN are known lachrymators.[17] The toxicity of the other PANs has not been studied though may be inferred from the relative toxicity of their precursors in the atmosphere. For example, given acrolein's higher toxicity relative to that of acetaldehyde,[18] APAN likely surpasses the potency of PAN (at least on a per-molecule basis).

In the lower troposphere, the removal of PANs is usually driven by thermal decomposition (TD; (R-2)), for example:

$$CH_2{=}CHC(O)O_2NO_2 + M \xrightarrow{\Delta} CH_2{=}CHC(O)O_2 + NO_2 + M,\ k_{-2} \quad (R\text{-}2)$$

Here, M indicates a "third body", *i.e.*, a pressure-dependent reaction. At atmospheric pressure, (R-2) follows first-order kinetics.[2] In the upper troposphere and at high latitudes, in contrast, the temperature (T) is sufficiently low for reaction with OH and photolysis to dominate as PAN removal pathways.[19] Near the ground in the surface boundary layer or within tree canopies, dry deposition including stomatal uptake[20–22] may also constitute a significant removal pathway.[2]

To correctly model the abundances of PANs and their impact in the troposphere, accurate knowledge of their TD kinetics is needed. Table 2 summarizes measured Arrhenius parameters for the TD of PAN, PPN, MPAN, and APAN. While the TD of PAN has been the subject of numerous studies, there have only been two studies of MPAN and only a single study of APAN (prior to this work). Grosjean *et al.*[31,36] investigated the TD of both compounds at T between 285 K and 300 K using samples generated *in situ* in a Teflon chamber. They reported activation energies that are quite different from the other PANs (in part due to a relatively narrow T range) and appear specious.[9] Furthermore, the MPAN data are inconsistent with measurements at $T > 302$ K by Roberts and Bertman.[27] Hence, corroboration of the TD parameters by Grosjean *et al.*[31,36] is warranted, especially for APAN for which no data at $T > 300$ K exist.

In this work, we studied the TD of APAN using a T-controlled flow reactor coupled to a gas chromatograph with an electron capture detector (PAN-GC) to monitor APAN concentrations. We report TD rate constants of APAN at T between 295.2 K and 320.7 K and at a pressure of (662 ± 11) torr and calculate Arrhenius parameters. To corroborate our results, we measured the TD of PAN at 313.2 K for which literature data are available.[27]

We also present ambient air measurements of PAN, PPN and APAN mixing ratios which were made at the Calgary Central (Inglewood) air quality station from April 17 to May 31, 2023, as part of the "Focus on nitrOgen diOxide at the Bird sAnctuaRy" (FOOBAR) campaign. From May 16 to May 21, elevated concentrations of carbon monoxide (CO), fine particulate matter ($PM_{2.5}$), and PANs were observed, associated with BB emissions that originated from several out-of-control wildfires to the north-northwest (NNW) of the measurement location. On several occasions, mixing ratios of PAN, PPN, and APAN decreased exponentially after sunset, allowing for an assessment of APAN loss rates in ambient air with the revised TD rates obtained in this work.

Table 2 Arrhenius parameters for the thermal decomposition of PAN, PPN, MPAN, APAN, and furoyl peroxynitrate (Fur-PAN) at atmospheric pressure selected from the literature

Molecule	A (s^{-1})	E_a (kJ mol^{-1})	k_{-2} (298 K) (10^{-4} s^{-1})	Reference
PAN	—	—	2.8 ± 0.8	23
PAN	$(0.8 \pm 1.1) \times 10^{15}$	104 ± 3	4.7	24
PAN	$(1.9 \pm 2.7) \times 10^{16}$	113 ± 4	3.7 ± 0.4	25
PAN	10^{18}	121 ± 8	5.4	26
PAN	3.16×10^{16}	113	4.9	27
PAN	2.52×10^{16}	112.85	4.17	28
PAN	1.21×10^{17}	101 ± 4	4.12 ± 0.25	29
PAN	—	—	3.1	30
PAN	$(2.5 \pm 2.3) \times 10^{17}$	119 ± 2	3.1	27
PAN	$(1.6 \pm 5.8) \times 10^{16}$	113 ± 9	3.0	31
PAN	$(0.5 \pm 1.3) \times 10^{16}$	109 ± 6	4.2	32
PAN	—	—	4.40 ± 0.13	33
PPN	2×10^{15}	106	4.4	34
PPN	$(1.6 \pm 4.7) \times 10^{25}$	164 ± 7	3.4	31
PPN	7.2×10^{16}	116 ± 2	3.5	35
PPN	—	—	3.67 ± 0.10	33
Fur-PAN	$(3.7 \pm 0.2) \times 10^{16}$	113.6 ± 4.2	4.6	7
MPAN	$(1.6 \pm 2.6) \times 10^{16}$	112 ± 4	3.5	27
MPAN	$(1.6 \pm 6.7) \times 10^{23}$	153 ± 10	2.3	36
APAN	$(0.3 \pm 4.1) \times 10^{20}$	131 ± 31	3.0	31
APAN	$(0.75 \pm 1.39) \times 10^{18}$	121.2 ± 4.8	4.3	This work

2. Methods

2.1 Synthesis of PANs

All chemicals were obtained from Sigma-Aldrich and used as received. In preliminary experiments, we attempted to generate APAN dynamically from photolysis of acryloyl chloride in the presence of NO_x.[37] However, in spite of previous success generating PAN, PPN or PiBN in high yield with 254 nm or 285 nm light sources,[38,39] we were unable to generate gas streams containing APAN in high purity by acryloyl chloride photolysis, as judged from the many, most likely chlorinated, byproducts that appeared in the chromatogram (not shown). Instead, APAN was synthesized and delivered from a diffusion source as described by Tokarek *et al.*[40] Briefly, 4.0 mL of acryloyl chloride was placed in an ice-cold 100 mL round bottom flask (RBF) containing a magnetic stirring bar. Cold hydrogen peroxide (50%, 1.5 mL) was then added dropwise, followed by 20.0 mL of cold tridecane. The RBF was then placed in an ice-water bath, and the mixture was stirred. Caution needs to be exercised at this stage as we observed, on one occasion, rapid and sudden gas evolution after ~1 h, resulting in some liquid splattering upwards and into the fume hood. After 2 hours, cold concentrated sulfuric (2.5 mL) and nitric acid (3.0 mL) were added dropwise, in turn. After 15 minutes, the organic and aqueous layers were separated in a pre-cooled 125 mL separatory funnel. The organic layer was washed three times with ~50 mL of cold deionized water, dried over magnesium sulfate, and filtered through glass wool. Aliquots of the synthesized APAN in tridecane solution were stored in 2.0 mL polypropylene centrifuge tubes (VWR) in a freezer prior to use. Once thawed, the APAN samples were generally less stable than those of other PANs and needed to be replaced on an approximately weekly schedule. In addition to APAN, batches of PAN were synthesized from acetic anhydride as described earlier.[40–42]

To corroborate the identity of APAN using relative elution times, gas streams containing PAN, PPN or PiBN were generated from photolysis at 285 nm of acetone, diethyl ketone, or diisopropyl ketone in the presence of NO_x as described previously.[39]

2.2 Measurement of TD kinetics in laboratory experiments

The experimental setup for the kinetics experiments is based on that described by Roberts and Bertman[27] and is shown in Fig. 1.

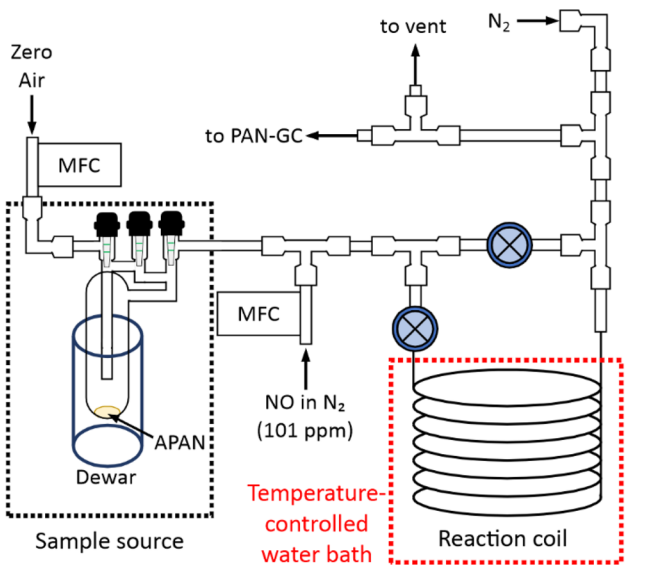

Fig. 1 Schematic of the experimental set-up (not to scale). MFC = mass flow controller.

A gas stream containing the PAN under investigation (*i.e.*, APAN or PAN) was delivered with "zero" air (>99.999% purity, Air Liquide ALPHAGAZ 1) using a 100 standard-cubic-centimeter-per-minute (sccm; calibrated to a temperature of 273.15 K and a pressure of 1 bar) capacity mass flow controller (MFC, MKS) from a Pyrex diffusion source maintained at 273.15 K. The diffusion source output was combined with a flow of ~15 sccm of 101 parts-per-million by volume (ppmv, 10^{-6}) of nitric oxide (NO) in O_2- and H_2O-free N_2 (Praxair) delivered *via* a 100 sccm capacity, all-metal MFC (MKS). The role of the NO is to rapidly titrate the APA or peroxyacetyl (PA) radicals to prevent the re-formation of PANs *via* (R2), for example:

$$CH_2{=}CHC(O)O_2 + NO \rightarrow CH_2{=}CHC(O)O + NO_2,\ k_3 \quad (R3)$$

The value of k_3 has not been experimentally determined for the reaction of NO with the APA radical but is likely of similar magnitude as that for NO + PA. Using the rate coefficient reported by Villalta and Howard[43] for reaction of the PA radical and NO, we calculate a PA and APA radical lifetime of <1 ms with respect to (R3) under our experimental conditions, *i.e.*, the re-formation of PANs *via* (R2) is calculated to be negligible.

The radical generated in (R3) dissociates to carbon dioxide (CO_2) and vinyl radical ($CH_2{=}CH$), which will react with O_2 to form formaldehyde (HCHO) and formyl radical (HCO),[44] which in turn reacts with O_2 to form carbon monoxide (CO) and hydroperoxyl radical (HO_2).[45] Under our experimental conditions, HO_2 is expected to be titrated by NO to form OH, which in turn is expected to react with NO or the inner walls of reaction vessel (rather than adding to the double bond of APAN and speeding up its decomposition).

Kinetic measurements were conducted using a reaction vessel constructed from ~1 cm outer diameter (o.d.) and ~0.8 cm inner diameter (i.d.) Pyrex glass that was double-coiled (12 revolutions downwards in an inner coil and another 12 revolutions on the outside back to the top) and submerged in a *T*-controlled water bath (Lauda Proline RP 1290, ±0.01 °C). The internal volume of this reaction vessel was (234 ± 2) mL, determined by measuring the volume of water needed to fill it. When not in use (*e.g.*, overnight), the reaction vessel and connecting tubing were continuously purged by a flow of ~5 sccm of zero air. Thermal decomposition in the connecting tubing outside and downstream of the heated vessel (internal volume ~5 cm^3) was estimated at ~0.1% and hence negligible.

The vessel effluent was combined with an always-on flow of 50 to 55 sccm of dry N_2 and analyzed by PAN-GC. The line pressure was monitored using a transducer (MKS Baratron 722A) mounted on the overflow vent line (not shown) and ranged from 650 torr to 671 torr (855 to 883 hPa).

Concentrations of PANs were monitored using a customized Hewlett-Packard (HP) 5890 PAN-GC described previously.[42] This GC was equipped with a 50 μL stainless steel sample loop and a 15 m long megabore analytical column (Restek RTX-200) with a film thickness of 1 μm. The GC was operated with N_2 carrier and make-up gas delivered from the "blow-off" of a liquid N_2 dewar. Injections were automated (and usually every 5 min). At a column flow rate of 15 mL min^{-1}, PAN, PPN and PiBN eluted at 110 s, 181 s, and 296 s, respectively, whereas APAN eluted at 163 s (Fig. S1A†). These relative elution order and times are consistent with those reported by Roberts *et al.*[9] who also used an RTX-200 column and with values by Tokarek *et al.*[40] who utilized a marginally more polar RTX-1701 column. Chromatographic peak areas were determined by fitting the parameters of a Gaussian expression to the observed peaks as described by Tokarek *et al.*[40]

Concentrations of APAN (or PAN) entering (C_0) and exiting (C_t) the reaction vessel were measured by manually bypassing the gas flow with the aid of 2-way valves (Swagelok PFA-43S4). The residence time (t_{res}), calculated by dividing the reactor volume by the total volumetric flow rate, was then systemically varied (Table S1†). In a typical experiment (Fig. 2), the reaction vessel was initially bypassed, and the PAN under investigation was eluted from the diffusion source. Once a stable (or only slowly changing) peak area (*i.e.*, concentration, C_0) was observed by the PAN-GC, the reaction coil was switched in-line to measure C_t and bypassed again after consecutive GC injections showed stable peak areas. Values of C_t/C_0 were calculated by dividing the peak areas observed with the reactor in-line (shown as red squares in Fig. 2) by a linear interpolation of the peak areas when the reactor was bypassed (shown as a blue line in Fig. 2). In the example shown in Fig. 2, C_t/C_0 equaled $0.54_4 \pm 0.01_4$, where the error is 1σ precision. The apparent loss rate constant (k') in the reaction coil was then obtained by linear regression from plots of $\ln\left(\frac{C_t}{C_0}\right)$ *versus* t_{res}.

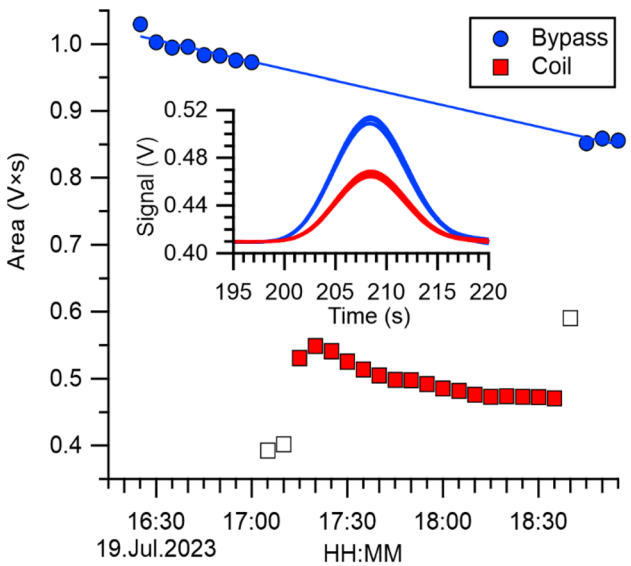

Fig. 2 Sample data collected in a representative experiment. In this example, the reaction coil was maintained at a temperature of (310.65 ± 0.01) K. The total volumetric flow rate through the coil was 64.4 mL min^{-1}, from which a residence time of 218 s was calculated. The circles (shown in blue colour) and squares (shown in red colour) show the APAN peak areas when the reaction coil was bypassed and inline, respectively. Data obtained during the transition between bypass and inline flows are shown as open symbols (□) were not considered in the analysis. The insert shows the corresponding chromatograms. The column flow rate was 15.0 mL min^{-1}.

Pyrex surfaces can destroy PANs, particularly at low humidity,[27,46] which adds to k':

$$k' = k_{-2} + k_{\text{Pyrex}}. \quad (1)$$

Here, k_{Pyrex} is the loss rate constant of APAN on the inner walls of the Pyrex coil. To probe the magnitude of k_{Pyrex}, experiments were conducted at room T (295.2 K) in which the gas stream entering the reactor was partially humidified by inserting a bubbler containing deionized water between the all-metal MFC delivering zero air and the Tee fitting connected to the sample source. Additional room-temperature experiments were carried out in which the Pyrex reaction coil was replaced with a ~50 cm Pyrex linear flow tube with 2.54 cm i.d. and ~270 cm^3 internal volume which was internally coated using halocarbon wax (Halocarbon LLC, series 1500).

For experiments at T < 300 K, TD rates were slow, necessitating long run times that made it challenging to maintain stable diffusion source outputs. In those cases, k' was calculated by dividing $-\ln\left(\frac{C_t}{C_0}\right)$ by t_{res} for individual experiments and averaging the results at each T. For experiments at T > 300 K, k' values were calculated from the slopes of plots of $\ln\left(\frac{C_t}{C_0}\right)$ *versus* t_{res}. At higher T, both approaches gave equivalent results (Table 3), with the second method being more precise.

To corroborate the results with APAN, we measured the TD rate of PAN at $T = 313.2$ K and compared to literature values. Complete lists of experiments conducted for APAN and PAN are shown in Tables S1 and S2,† respectively.

Rates for TD reactions are commonly shown in the form of an Arrhenius plot, *i.e.*, of $\ln(k_{-2})$ *versus* $1/T$. In this work, the k' data were fit to the parameters of a rearranged Arrhenius expression:

$$\ln\left(k'\right) \approx \ln(k_{-2}) = \ln(A) - \frac{E_a}{R}\left(\frac{1}{T}\right) \quad (2)$$

Here, A is the Arrhenius pre-exponential factor, E_a is the activation energy in kJ mol^{-1}, and R is the universal gas constant (8.314 J mol^{-1} K^{-1}).

2.3 Observations of APAN in ambient air

Ambient air mixing ratios of PAN, PPN, and APAN were measured by PAN-GC as part of the "Focus on nitrOgen diOxide at the Bird sAnctuaRy" (FOOBAR) campaign, which took place in Calgary from March 20 to May 31, 2023. The PAN-GC was a Varian 3380 CP modified and operated in a similar fashion as described by Tokarek *et al.*[40] This instrument was equipped with a 500 μL stainless steel sample loop and a 30 m long megabore column (Restek RTX-1701; film thickness 1 μm) maintained at 298.2 K. It was operated with high purity (99.999%) helium carrier gas at a flow rate of 19.1 mL min^{-1} (increased to 37.4 mL min^{-1} on May 8), N_2 make-up gas at a flow of 13.2 mL min^{-1}, an electron capture detector T of 100 °C, and the "N_2 high" sensitivity setting. The instrument response factors for PAN and PPN were determined using photochemically generated gas mixtures calibrated against blue diode thermal dissociation cavity ring-down spectroscopy (TD-CRDS) as described by Rider *et al.*[39] The response factor for APAN was calculated from the relative APAN:PAN response factor measured by Tokarek *et al.*[40] A sample ambient air chromatogram is shown in Fig. S1B.† The instrument reported 10 min data from April 17 to May 31, 2023.

Auxiliary measurements included mixing ratios of NO_2 and ΣPAN by TD-CRDS,[47] NO, total odd nitrogen (NO_y) and O_3 using commercial NO–O_3 chemiluminescence and absorption analyzers (Thermo Scientific 42i-Y and 49i), and meteorological

Table 3 First-order rate constants for loss of APAN (k') as a function of temperature (T). n is the number of experiments at each T. The second from right column contains Pearson correlation coefficients (r) when k' values were derived from linear fits of $\ln\left(\frac{C_t}{C_0}\right)$ *versus* t_{res} (Fig. 3). Stated uncertainties are at the 1σ precision level. n/d = not determined

Reference	T (K)	n	k'^a (10^{-5} s^{-1})	k'^b (10^{-5} s^{-1})	r	$k_{-2}{}^c$ (10^{-5} s^{-1})
This work	320.7	6	1336 ± 20	1334 ± 9	99.98%	1306 ± 9
This work	318.2	6	968 ± 53	958 ± 17	99.8%	930 ± 17
This work	315.2	6	674 ± 67	680 ± 20	99.6%	652 ± 20
This work	313.2	7	534 ± 50	527 ± 14	99.6%	499 ± 14
This work	310.7	8	364 ± 58	352 ± 20	97.7%	324 ± 20
This work	308.2	8	230 ± 37	228 ± 13	97.7%	200 ± 13
This work	303.2	6	137 ± 30	130 ± 15	94.8%	102 ± 15
This work	295.2	2	63 ± 2	n/d	n/d	n/d
This work[d]	295.2	4	51 ± 4	51 ± 2	99.6%	n/d
Grosjean *et al.*[31]	299.1	1				67.0 ± 12.9
Grosjean *et al.*[31]	297.8	1				29.9 ± 2.5
Grosjean *et al.*[31]	293.2	1				8.3 ± 0.2
Grosjean *et al.*[31]	293.2	1				8.3 ± 0.2
Grosjean *et al.*[31]	290.2	1				6.5 ± 0.5
Grosjean *et al.*[31]	290.2	1				7.7 ± 0.4

[a] Average and standard deviation of k_{-2} values calculated in individual experiments (Table S1). [b] Derived from linear fits of $\ln\left(\frac{C_t}{C_0}\right)$ *versus* t_{res} (Fig. 3). [c] $k_{\text{Pyrex}} = 2.8 \times 10^{-4}$ s^{-1} subtracted (see text). [d] Experiments conducted with humidified zero air and Teflon-coated linear flow reactor.

data collected using a commercial sensor (Vaisala WXT520). All instruments sampled from the same height, ~4.5 m above ground.

The instruments were housed in a mobile laboratory parked adjacent to the Calgary Central (Inglewood) air quality station located at 51° 1′ 47.7840″ North Latitude and 114° 0′ 29.1996″ West Longitude and operated under the guidance of the Calgary Region Airshed Zone (CRAZ), a non-profit association with members from government agencies (federal, provincial, and municipal), non-government organizations, industry, and the public. The Inglewood station houses several continuously operated instruments, including a commercial carbon monoxide (CO) infrared analyzer (Thermo Scientific 48i) and a real-time particulate monitor (Thermo Scientific 5030 SHARP) quantifying sub-2.5 μm aerosol mass ($PM_{2.5}$).

3. Results

3.1 Laboratory studies

An overview of the experiments conducted is given in Tables S1 (for experiments with APAN) and S2 (for experiments with PAN).† For each experiment, a value for k_{-2} was calculated by dividing $-\ln\left(\frac{C_t}{C_0}\right)$ by t_{res} (Tables S1 and S2†). Averages and standard deviations of these values for APAN at each T are summarized in Table 3 under the column heading k'^a. Alternatively, values of k_{-2} were calculated, by linear regression with forced "zero" intercept, from the slopes of plots of $\ln\left(\frac{C_t}{C_0}\right)$ against t_{res} at each T (Fig. 3); these results are summarized in Table 3 under the column heading k'^b and were consistent with the first method though more precise, with a relative standard deviation ranging from 0.7% at 320.7 K to 11.7% at 303.2 K. The absence of curvature in the plots shown in Fig. 3, judged from their large Pearson correlation coefficients (r) of typically >99% (Table 3) indicates that the APAN decay rate was not affected by secondary chemistry arising from $CH_2{=}CHC(O)O$ that is generated by (R3).

To probe whether the Pyrex walls contributed to the apparent APAN loss in our experiments, experiments were conducted at 295.2 K using humidified flows and with an internally Teflon-coated flow reactor. These experiments yielded lower k' values than those obtained with the reaction coil and the dry zero air, $(51 \pm 4) \times 10^{-5}$ s^{-1} *versus* $(63 \pm 2) \times 10^{-5}$ s^{-1} (Table 3), confirming that APAN indeed is partially scrubbed on the inner walls of the Pyrex reactor. A lower limit for k_{Pyrex} of $\geq 1.2 \times 10^{-4}$ s^{-1} was calculated from the difference of the value with and without Teflon. This value is a lower limit as humidification and the Teflon coating may not fully eliminate wall losses.

The reactor wall loss contributes to all experiments but will have a lesser impact at the higher T where it is not as fast as TD and hence TD dominates. With the assumption that k_{Pyrex} is not T-dependent, we estimated its magnitude from r values of plots of $\ln(k' - k_{Pyrex})$ *versus* $\left(\frac{1}{T}\right)$ in the 303.2–320.7 K T range as a function of k_{Pyrex} (not shown). A maximum r value of 0.996 was observed at $k_{Pyrex} = 2.8 \times 10^{-4}$ s^{-1}. This value was subtracted from all k' values to calculate k_{-2}; the results are summarized in Table 3 under the column heading $k_{-2}{}^c$. These values are plotted in Fig. 4 and were fitted to eqn (1), with the results of the fit shown in Table 2. By extrapolation, a loss rate constant of $k_{-2} = 4.3 \times 10^{-4}$ s^{-1} at $T = 298$ K was calculated, in excellent agreement with k_{-2} (298 K) of other PANs (Table 2). In contrast, the same analysis with assumed $k_{Pyrex} = 1.2 \times 10^{-4}$ s^{-1} gave

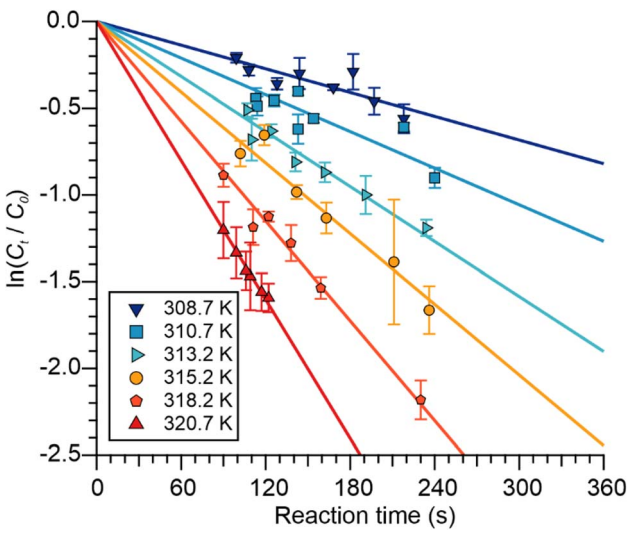

Fig. 3 Plots of $\ln(C_t/C_0)$ for APAN *versus* t_{res} (*i.e.*, reaction time) as a function of reactor temperature. Error bars are at the 1σ precision level.

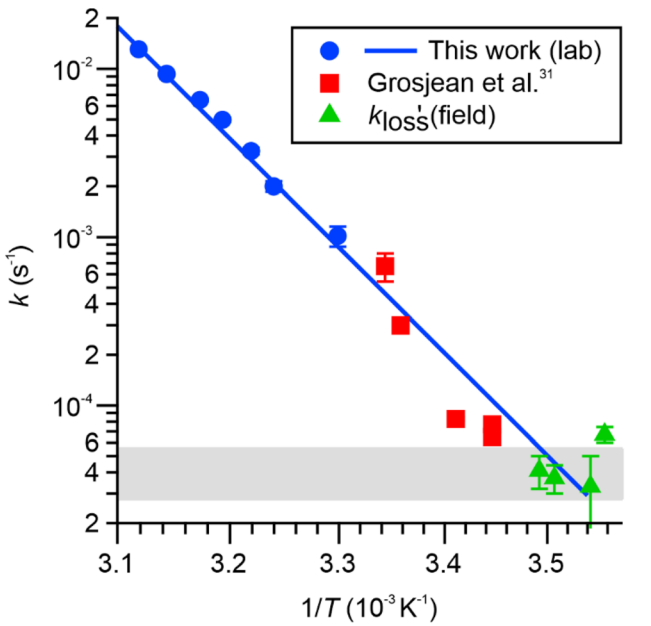

Fig. 4 Arrhenius plot of k_{-2} (blue circles) *versus* $1/T$ for APAN. Error bars for the laboratory data shown are $\pm 1.4 \times 10^{-4}$ s^{-1} ($\frac{1}{2}$ of the magnitude of k_{Pyrex}). Data from Grosjean *et al.*[31] and pseudo-first order loss rate constants derived from ambient air data are shown as red squares and green triangles, respectively. The grey bar indicates the range of dry deposition loss rates for PAN reported by Roberts.[2]

k_{-2} (298 K) of 5.1×10^{-4} s^{-1}, which would be inconsistent with other PANs.

For PAN, we measured $k' = (3.3 \pm 0.1) \times 10^{-3}$ s^{-1} at $T = 313.2$ K (Table S2 and Fig. S2†). Subtracting $k_{\text{Pyrex}} = 2.8 \times 10^{-4}$ s^{-1} yields $k_{-2} = (3.0 \pm 0.1) \times 10^{-3}$ s^{-1}, in excellent agreement with the value of $(2.9 \pm 0.5) \times 10^{-3}$ s^{-1} reported by Roberts[27] at that T.

3.2 Ambient air observations of PAN, PPN and APAN in BB plumes

A time series of ambient air observations from May 16, midnight, to May 21, noon, local or mountain daylight time (MDT), 2023, is shown in Fig. 5. On the morning of May 16, the city of Calgary was blanketed by a BB plume, as indicated by a sudden increase of CO and $PM_{2.5}$ abundance, which peaked at 2.9 ppmv and 450 μg m^{-3}, respectively. The smoke originated from several out-of-control wildfires burning to the NNW of the measurement location (Fig. S3†), including the Grizzly Complex wildfire south of Slave Lake which forced an evacuation of the town of Swan Hills in Northern AB on May 16. Media reports described the air quality in Calgary as "among the worst in the world", "while the thick haze gave off an acrid smell, glowed orange and reduced visibility to half a mile".[48] Downwind, the wildfire emissions generated record-breaking O_3 anomalies across the U.S. upper Midwest,[49] and measurable health effects were reported as far away as New York City.[50]

Mixing ratios of PAN, PPN, and APAN were elevated during this event, peaking at 3.4 ppbv, 455 pptv, and 220 pptv, respectively. These data are amongst the highest mixing ratios of BB-generated APAN reported at a surface site to date (Table 1) and are the largest mixing ratios measured by this research group.[40] Prior to (and after) the BB event, APAN mixing ratios were <10 pptv. In the plume, the APAN:PAN ratio ranged from 4% to 8% (Fig. S4†), which is a larger ratio than reported in other BB studies though smaller than APAN:PAN ratios associated with industrial sources (Table 1). Average ratios of PPN to PAN and APAN to PAN mixing ratios were 12.5% and 6.0%, respectively (Fig. S4†).

In addition to the period shown in Fig. 5, BB smoke was observed on the morning of May 22 as well as from May 24 to May 28, 2023 (data not shown). During those times, PAN, PPN, and APAN mixing ratios peaked at 1.15 ppbv, 200 pptv, and 40 pptv, respectively, and CO and $PM_{2.5}$ peaked at 602 ppbv and 47 μg m^{-3}, respectively.

3.3 APAN loss rate constants derived from ambient air data

Mixing ratios of the PANs generally increased during daytime, when PANs are photochemically produced, and decreased

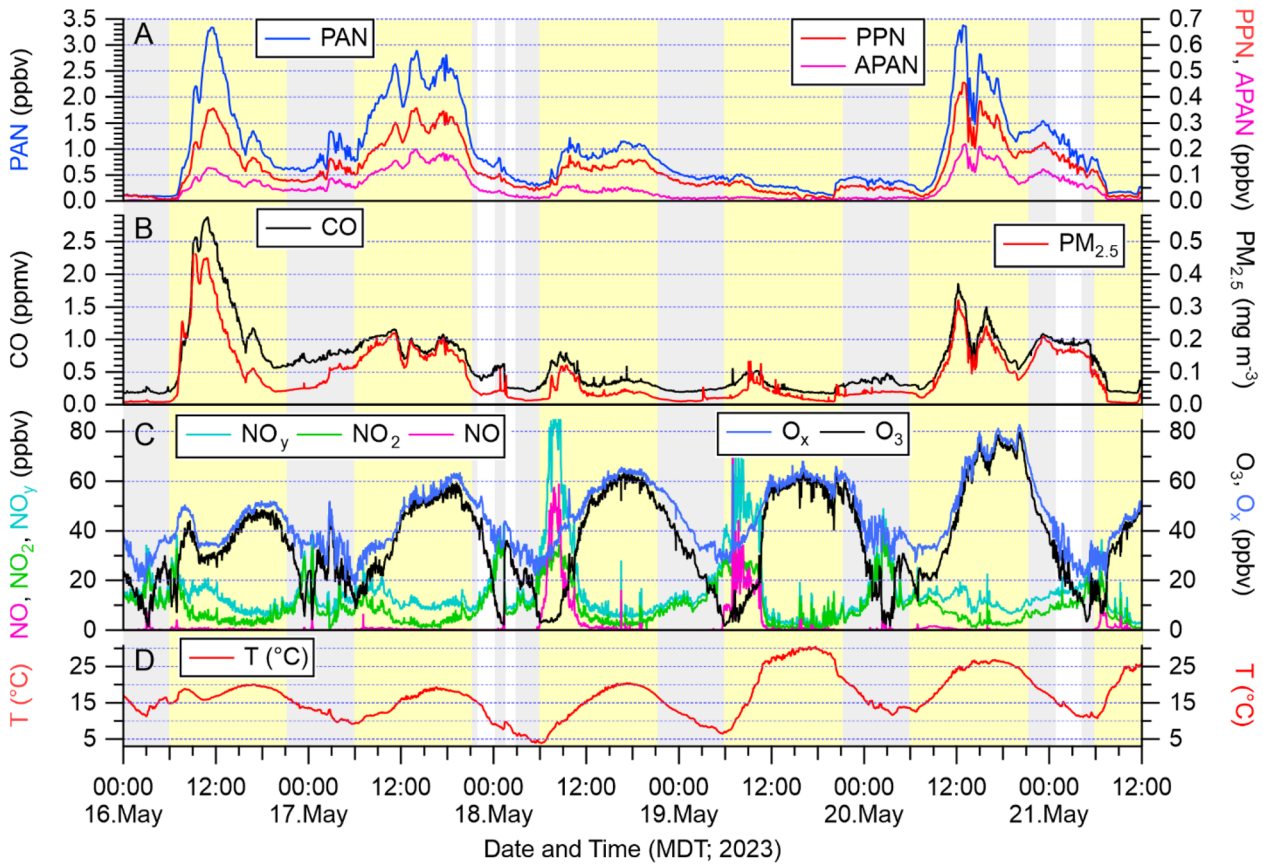

Fig. 5 Partial time series of quantities measured during FOOBAR. (A) PAN (left axis) and PPN and APAN (right axis). (B) Carbon monoxide (CO; left axis) and $PM_{2.5}$ (right axis). (C) Nitric oxide (NO), nitrogen dioxide (NO_2) and total odd nitrogen (NO_y; left axis), and ozone (O_3) and odd oxygen ($O_x = O_3 + NO_2$; right axis). (D) Ambient air temperature. The background shading indicates night (light gray) and day (light yellow). Regions shaded in white colour were selected for further analysis (see text).

Table 4 Overview of periods during FOOBAR selected for estimation of k'_{loss} for PANs in ambient air. LOQ = limit of quantification (~50 pptv for NO). Times are mountain daylight time (MDT). Errors denote $\pm 1\sigma$ precision

Quantity\Period	May 17 22:00–midnight	May 18 01:40–02:40	May 21 01:00–04:00	May 25–May 26 23:30–02:50
PAN_0 (pptv)	815	511	1222	762
PPN_0 (pptv)	106	69	174	113
$APAN_0$ (pptv)	47	24	89	22
NO (pptv)	<LOQ	<LOQ	<LOQ	<LOQ
NO_2 (ppbv)	14.1 ± 3.5	7.0 ± 0.5	10.4 ± 1.4	16.8 ± 3.8
NO_y (ppbv)	16.5 ± 3.5	9.1 ± 0.5	16.1 ± 1.5	18.9 ± 3.8
O_3 (ppbv)	31.3 ± 8.0	29.5 ± 4.5	20.4 ± 5.6	18.3 ± 5.9
$P(NO_3)$ (ppb h^{-1})	0.77 ± 0.10	0.35 ± 0.06	0.41 ± 0.13	0.47 ± 0.15
RH (%)	44 ± 10	52 ± 5	64 ± 8	75 ± 6
CO (ppbv)	436 ± 36	256 ± 5	943 ± 26	409 ± 18
$PM_{2.5}$ ($\mu g\ m^{-3}$)	33.4 ± 2.3	21.0 ± 2.6	164.3 ± 3.7	23.2 ± 1.3
T (°C)	12.0 ± 2.0	8.0 ± 1.1	13.2 ± 1.3	9.1 ± 1.2
k_{-2} (PAN)[a]	5.6×10^{-5} s^{-1}	2.9×10^{-5} s^{-1}	6.9×10^{-5} s^{-1}	3.5×10^{-5} s^{-1}
k_{-2} (PPN)[a]	4.7×10^{-5} s^{-1}	2.4×10^{-5} s^{-1}	5.7×10^{-5} s^{-1}	2.9×10^{-5} s^{-1}
k_{-2} (APAN)[b]	4.7×10^{-5} s^{-1}	2.3×10^{-5} s^{-1}	5.9×10^{-5} s^{-1}	2.8×10^{-5} s^{-1}
k'_{loss}(PAN)	$(3.5 \pm 0.4) \times 10^{-5}$ s^{-1}	$(6.7 \pm 1.0) \times 10^{-5}$ s^{-1}	$(4.6 \pm 0.9) \times 10^{-5}$ s^{-1}	$(3.5 \pm 0.5) \times 10^{-5}$ s^{-1}
r	0.948	0.968	0.785	0.853
k'_{loss}(PPN)	$(3.6 \pm 0.4) \times 10^{-5}$ s^{-1}	$(7.0 \pm 0.2) \times 10^{-5}$ s^{-1}	$(3.8 \pm 0.8) \times 10^{-5}$ s^{-1}	$(3.2 \pm 0.5) \times 10^{-5}$ s^{-1}
r	0.939	0.9991	0.780	0.862
k'_{loss}(APAN)	$(3.7 \pm 0.7) \times 10^{-5}$ s^{-1}	$(6.2 \pm 0.7) \times 10^{-5}$ s^{-1}	$(4.1 \pm 0.9) \times 10^{-5}$ s^{-1}	$(3.3 \pm 1.7) \times 10^{-5}$ s^{-1}
r	0.862	0.981	0.767	0.485
$k'_{loss}(O_x)$	$(4.8 \pm 0.2) \times 10^{-5}$ s^{-1}	$(9.8 \pm 0.6) \times 10^{-5}$ s^{-1}	$(4.3 \pm 0.3) \times 10^{-5}$ s^{-1}	$(4.2 \pm 0.2) \times 10^{-5}$ s^{-1}

[a] Calculated based on values by Kabir *et al.*[33] [b] Based on laboratory experiments in this work.

starting in the late afternoon and into the night when the photochemical production of PA radicals (*e.g.*, from reaction of OH and aldehydes) diminishes (Fig. 5). The time periods after sunset thus provided an opportunity to probe PAN loss kinetics. In addition to chemical production and loss, ambient air mixing ratios may have also increased or decreased due to air mass shifts, *i.e.*, changes in BB plume intensity. Using seemingly stable concentrations of CO and $PM_{2.5}$ as an initial guide, nocturnal time periods showing pseudo-first order exponential decay in the APAN mixing ratio were selected for further analysis (Table 4); three of these periods are indicated with a white background in Fig. 5. Concentrations of CO and $PM_{2.5}$ concentrations were nearly constant during those selected times, suggesting that loss of PAN, PPN, and APAN was likely not due to transport, *i.e.*, not a result of shifting air masses. In all cases, NO mixing ratios were below our ability to quantify (*i.e.*, less than the limit of quantification if ~50 pptv). Further, NO_2 and O_3 mixing ratios were sufficiently large to sustain a nitrate radical (NO_3) production rate, calculated from $k_4[NO_2][O_3]$,[51] of between 0.35 and 0.77 ppb h^{-1}.

$$NO_2 + O_3 \rightarrow NO_3 + O_2,\ k_4 \qquad \text{(R4)}$$

For the selected cases, plots of $\ln(C_0/C_t)$ *versus* time were linear as judged from their r values (Fig. S5† and Table 4). Further, PAN, PPN, and APAN decayed in unison (Fig. 5) with statistically identical values of their apparent loss rate coefficients (k'_{loss}) during each episode (Table 4).

The k'_{loss} values for PAN and PPN were compared to k_{-2} values calculated using the parameterization by Kabir *et al.*[33] The k'_{loss} values for APAN are superimposed in Fig. 4 for comparison with k_{-2} predicted from the laboratory parameterization determined in this work. In all cases, the k'_{loss} values were of the same order of magnitude as k_{-2}. The apparent loss rates were ~1/3 slower than the predicted k_{-2} on May 17 and May 21 and equal to the k_{-2} on May 26. For the May 18 data, however, the rate constants derived from the scatter plot shown in Fig. S5† were three times as large as the predicted k_{-2} value.

Mixing ratios of odd oxygen ($O_x = O_3 + NO_2$) also decreased with first-order exponential kinetics and rate constants between 4.2×10^{-5} and 9.8×10^{-5} (Table 4), factors between 0.9 and 1.5 larger than those determined for the PANs. Mixing ratios of O_x were chosen (as opposed to O_3) to account for titration of O_3 by NO to NO_2.

4. Discussion

4.1 Laboratory measurements

This work constitutes only the second investigation of the TD kinetics of APAN reported in the literature. The first study was that by Grosjean *et al.*[31] who reported k_{-2} values in the range 290 K ≤ T ≤ 299 K, whereas this study covered the 303.2 K ≤ T ≤ 320.7 K range (Table 3). As is evident from Fig. 4, our data leads to a revised Arrhenius expression with an activation barrier that is lower than that reported by Grosjean *et al.*,[31] (121 ± 5) kJ mol^{-1} *versus* (139 ± 6) kJ mol^{-1}, and is more in line with values reported for other PANs (Table 2). We believe our data to be more accurate than the values by Grosjean *et al.*[31] as our results are corroborated by the good agreement of our measured k' and k_{-2} values for PAN with literature (Fig. S2†). It is also worth noting that the study by Grosjean *et al.*[31] encompassed only four data points over a narrow T range, a limitation noted by

Grosjean *et al.*[31] themselves; it is hence not surprising that their Arrhenius parameters would differ from one derived from data collected over a wider T range (Table 2). Furthermore, our data are more linear ($r = 0.992$) than the data reported by Grosjean *et al.*[31] which appear more scattered (Fig. 4). Finally, the discrepancy echoes what had occurred for MPAN, for which Grosjean *et al.*[36] reported an E_a value of (153 ± 10) kJ mol^{-1} in contradiction with Roberts and Bertman[27] who reported (112 ± 4) kJ mol^{-1}.

However, there is a fundamental difference between the two studies: the experimental approach. Grosjean *et al.*[31] utilized a Teflon smog chamber and generated APAN *in situ* using sunlight, acrolein, and NO, whereas we utilized a glass reaction coil and an APAN diffusion source. Following APAN generation, their chamber would have contained a considerable amount of NO_2, which increases the effective lifetime of APAN (eqn (3)) as the TD fragments would have had a reasonable chance to recombine rather than react with NO. The apparent PAN loss rate constant (k'_{loss}) under these conditions is

$$k'_{loss} = k_{-2}\left(\frac{k_{loss}(PA)}{k_{loss}(PA) + k_2[NO_2]}\right) \leq k_{-2}, \quad (3)$$

where k_{loss} (PA) is the pseudo-first order rate coefficient for loss of the PA radical.[28,32] In our laboratory experiments (Section 3.1), k_{loss} (PA) is equal to k_3[NO] and large because NO was deliberately added in high concentration. Grosjean *et al.*[31] were aware of this and monitored NO_2 concentrations but did not provide details as to the magnitude of the correction applied. As such, the kinetic parameter needed to make this correction, k_2, has not been measured for the APA radical and is hence somewhat uncertain, an uncertainty that would have added to their measurements.

In contrast to the smog chamber studies by Grosjean *et al.*,[31,36] the study by Roberts and Bertman[27] and this work utilized a Pyrex reactor to dissociate PANs. These experimental setups suffer from a potential bias: We observed that APAN decomposes faster on dry Pyrex surfaces than on either humidified or Teflon-coated Pyrex, necessitating a correction by $k_{Pyrex} = 2.8 \times 10^{-4}$ s^{-1}, assumed to be T-independent. An outstanding question is why the decomposition of APAN is faster on dry than on humidified Pyrex as has been reported for other PANs.[27,46] Theoretical studies, *e.g.*, by density functional theory,[52] are needed to probe and rationalize the role of water in the TD of PANs on Pyrex surfaces.

The choice of k_{Pyrex} limits the accuracy of our study: For example, if we assume a value of $k_{Pyrex} = 1.2 \times 10^{-4}$ s^{-1} (the minimum value at $T = 295.2$ K), we would have obtained $k_{-2} = 10^{(16.9\pm0.8)} e^{-(115.1\pm4.6)\ \text{kJ mol}^{-1}/(RT)}$ s^{-1} and k_{-2} (298 K) $= 5.1 \times 10^{-4}$ s^{-1} which are quite different from the values calculated with $k_{Pyrex} = 2.8 \times 10^{-4}$ s^{-1} that are shown in Table 2. Even so, our kinetic data are corroborated by observations made with heated instrument inlets. For example, Veres and Roberts[37] reported APAN to have TD kinetics of similar magnitude as those of the other PANs. Overall, a consistent picture emerges: The TD parameters for all PANs fall in the ranges of 106 kJ mol^{-1} < E_a < 122 kJ mol^{-1} and 2.8×10^{-4} s^{-1} < k_{-2} (298 K) < 4.6×10^{-4} s^{-1} (if studies published before the year 1980 are omitted). This makes sense chemically, as the TD rate is mainly determined by the strength of the –O–NO_2 bond, and the nature of the side chain would be of lesser importance. Only the values reported by Grosjean *et al.*[31,36] fall outside those ranges (Table 2).

4.2 Field measurements and atmospheric significance

The large PAN, PPN and APAN mixing ratios observed in this study highlights the importance of this class of compounds as the abundances of these lachrymators is set to increase with global climate change, which increases the frequency and severity of BB events. The data presented in this manuscript inform about APAN emission factors from BB plumes *via* APAN:PAN and PPN:PAN ratios (Fig. S4†) as well as ratios with respect to NO_y (Table 4).

As such, the ambient air observations provided a fortuitous opportunity to evaluate the revised parameterization for TD of APAN from this paper's laboratory experiments under "real-world" conditions. During the periods selected, the mixing ratios of PAN, PPN and APAN decreased with identical pseudo-first order rate constants, k'_{loss}. Further, the observed k'_{loss} values appear to agree (within error limits) with k_{-2} values predicted using laboratory parameterizations (Table 4 and Fig. 4). For APAN, this parameterization was extrapolated from the T range of our lab experiments (295.2–320.7 K) to that of the ambient air data (280–287 K).

At first glance, this seems like an excellent result. However, because of these relatively cool temperatures, the lifetimes of the PANs with respect to TD was relatively long, making it possible for other loss pathways to dominate. Further, for TD to dominate the atmospheric removal loss of PANs, the generated PA radicals need to be removed, and quickly. For the four ambient air periods selected, the NO mixing ratios were below our ability to quantify (*i.e.*, <50 pptv), in contrast to the laboratory experiments (Section 3.1), where k_{loss} (PA) was fast because NO was deliberately added in high concentration. It is unclear which reaction(s), if any, other than (R3) would have removed PA radicals and to what extent. Potential candidates for PA radical removal include aerosol uptake,[53] and reaction with NO_3 (ref. 54) or with organic peroxy radicals, XO_2.[22,55] Villalta *et al.*[53] reported a relatively large uptake coefficient (γ) of 0.0043 for uptake of $CH_3C(O)O_2$ radicals on deionized water at 274 K, and the aerosol surfaces in the BB plume, while not quantified, were likely large. Thus, aerosol uptake of PA radicals was likely their largest sink. Still, one would expect that reaction of PA radicals with NO_2 (R2) would have increased the apparent lifetime of the PANs (eqn (3)), *i.e.*, the apparent loss rate constitutes a lower limit to k_{-2}. Perhaps not surprisingly then, the field data (shown as green triangles in Fig. 4) tend to fall below the linear fit of the TD rate extrapolated from higher T data.

Another assumption of this analysis is that nocturnal sources of PANs such as reactions of NO_3 with aldehydes[54] were negligible. Neither mixing ratios of NO_3 nor those of VOCs (from which NO_3 abundances could be constrained) were quantified during FOOBAR. Nevertheless, the instantaneous NO_3 production rate, P(NO_3), was large during the selected

periods, 0.35 to 0.77 ppbv h^{-1} (Table 4), which is within the range of 0.1 to 1.5 ppbv h^{-1} reported by Decker *et al.*[56] who observed nocturnal BB plumes from an aircraft platform. Thus, all of the selected periods were conducive to NO_3 formation. However, Decker *et al.*[56] also noted exceptionally large total NO_3 reactivity toward BB-VOCs of between 17 and 70 s^{-1} that only gradually decreased during the several hours transport time between the emission source and observation point. Large NO_3 sinks were likely also present during the BB events in this data set, implying that NO_3 mixing ratios would have been small during those times. How much chemistry went through the NO_3 + aldehyde channel (which can yield PANs) during FOOBAR is unclear.

Finally, the analysis assumes that direct sinks of PANs (other than TD followed by removal of the PA radicals) such as aerosol uptake[57] and dry deposition[20–22] were also negligibly small. Lifetimes of PAN with respect to dry deposition have been estimated to be in the 5–10 h range,[2] which translate to a loss rate constant of between 5.6×10^{-5} s^{-1} to 2.8×10^{-5} s^{-1}, which is on par with the k'_{loss} values determined in this work (Table 4). In this context, the O_x loss constants, $k'_{loss}(O_x)$, are informative since deposition velocities (v_d) for O_3 are of similar magnitude (with a range of 0.1 to 0.7 cm s^{-1})[58] as those of PAN, for which v_d values between 0.13 and 0.54 cm s^{-1} have been reported.[2] The values of $k'_{loss}(O_x)$ are slightly larger than k'_{loss} of the PANs, which supports the notion that both O_3 and PANs are removed mainly by dry deposition. However, Decker *et al.*[56] reported a total O_3 reactivity toward BB-VOCs of up to $\sim 6 \times 10^{-4}$ s^{-1} which rapidly decreased with plume age to $\sim 2 \times 10^{-4}$ s^{-1}, about a factor of two to four larger than $k'_{loss}(O_x)$ in this work. In other words, the observed O_x loss could have entirely been due to chemical reactions as opposed to dry deposition; in the absence of speciated VOC, it is not possible to tell. For APAN, the implication is that the nocturnal losses are explained through a combination of dry deposition and TD.

5. Conclusions

The laboratory experiments have yielded revised and more accurate parameterization of the TD kinetics for APAN than previously reported by Grosjean *et al.*[31] Large APAN mixing ratios were observed in ambient air during a spring BB episode. The ambient air temperatures were ultimately too cold to allow for additional constraints of the TD kinetics of APAN as other sinks (*e.g.*, dry deposition) were competitive. Overall, analysis of field data should not be construed as a substitute for properly conducted laboratory studies.

Data availability

Data supporting the laboratory experiments described in this article have been included as part of the ESI.† Data supporting the field experiments are available at **https://doi.org/10.5683/SP3/VXLT6V** (after acceptance). During review, please use the following URL for anonymous access: Private URL: **https://borealisdata.ca/privateurl.xhtml?token=eab128af-bdc4-4ad7-8905-6a01bbb9b077**.

Author contributions

NMJ and KDE synthesized the APAN samples. NMJ, ALG, and KDE carried out the experiments and reduced the data. ALG, KDE, and SJ acquired ambient air data. HDO conceptualized the experiments and drafted the manuscript.

Conflicts of interest

There are no conflicts of interest to declare.

Acknowledgements

This work was made possible by the financial support of the Natural Sciences and Engineering Research Council of Canada (NSERC) in the form of a Discovery grant to HDO (RGPIN-2022-03128). KDE acknowledges an NSERC undergraduate student research award (USRA). Acquisition of ambient air data was supported by Alberta Environment and Protected Areas. The authors thank the Calgary Region Airshed Zone (CRAZ) for providing access to and power at the Calgary Central (Inglewood) AQ station and time-resolved CO and $PM_{2.5}$ data. Partial funding for the FOOBAR study was provided by a grant from Alberta Environment and Protected Areas (23GRRSD63).

References

1 J. M. Roberts, The atmospheric chemistry of organic nitrates, *Atmos. Environ., Part A*, 1990, **24**, 243–287.
2 J. M. Roberts, in *Volatile Organic Compounds in the Atmosphere*, ed. R. Koppmann, Blackwell Publishing, Oxford, UK, 2007, pp. 221–268.
3 J. S. Gaffney and N. A. Marley, The Impacts of Peroxyacetyl Nitrate in the Atmosphere of Megacities and Large Urban Areas: A Historical Perspective, *ACS Earth Space Chem.*, 2021, **5**, 1829–1841.
4 J. M. Roberts, B. T. Jobson, W. Kuster, P. Goldan, P. Murphy, E. Williams, G. Frost, D. Riemer, E. Apel, C. Stroud, C. Wiedinmyer and F. Fehsenfeld, An examination of the chemistry of peroxycarboxylic nitric anhydrides and related volatile organic compounds during Texas Air Quality Study 2000 using ground-based measurements, *J. Geophys. Res.*, 2003, **108**, 4495.
5 W. Zheng, F. M. Flocke, G. S. Tyndall, A. Swanson, J. J. Orlando, J. M. Roberts, L. G. Huey and D. J. Tanner, Characterization of a thermal decomposition chemical ionization mass spectrometer for the measurement of peroxy acyl nitrates (PANs) in the atmosphere, *Atmos. Chem. Phys.*, 2011, **11**, 6529–6547.
6 Y. Lee, L. G. Huey, Y. Wang, H. Qu, R. Zhang, Y. Ji, D. J. Tanner, X. Wang, J. Tang, W. Song, W. Hu and Y. Zhang, Photochemistry of Volatile Organic Compounds in the Yellow River Delta, China: Formation of O_3 and Peroxyacyl Nitrates, *J. Geophys. Res.: Atmos.*, 2021, **126**, e2021JD035296.
7 J. M. Roberts, J. A. Neuman, S. S. Brown, P. R. Veres, M. M. Coggon, C. E. Stockwell, C. Warneke, J. Peischl and

M. A. Robinson, Furoyl peroxynitrate (fur-PAN), a product of VOC–NOx photochemistry from biomass burning emissions: photochemical synthesis, calibration, chemical characterization, and first atmospheric observations, *Environ. Sci.: Atmos.*, 2022, **2**, 1087–1100.

8 H. Tanimoto and H. Akimoto, A new peroxycarboxylic nitric anhydride identified in the atmosphere: CH_2=CHC(O)OONO_2 (APAN), *Geophys. Res. Lett.*, 2001, **28**, 2831–2834.

9 J. M. Roberts, F. Flocke, A. Weinheimer, H. Tanimoto, B. J. Jobson, D. Riemer, E. Apel, E. Atlas, S. Donnelly, V. Stroud, K. Johnson, R. Weaver and F. C. Fehsenfeld, Observations of APAN during TexAQS 2000, *Geophys. Res. Lett.*, 2001, **28**, 4195–4198.

10 Z. C. J. Decker, K. J. Zarzana, M. Coggon, K.-E. Min, I. Pollack, T. B. Ryerson, J. Peischl, P. Edwards, W. P. Dubé, M. Z. Markovic, J. M. Roberts, P. R. Veres, M. Graus, C. Warneke, J. de Gouw, L. E. Hatch, K. C. Barsanti and S. S. Brown, Nighttime Chemical Transformation in Biomass Burning Plumes: A Box Model Analysis Initialized with Aircraft Observations, *Environ. Sci. Technol.*, 2019, **53**, 2529–2538.

11 Y. R. Lee, L. G. Huey, D. J. Tanner, M. Takeuchi, H. Qu, X. X. Liu, N. L. Ng, J. H. Crawford, A. Fried, D. Richter, I. J. Simpson, D. R. Blake, N. J. Blake, S. Meinardi, S. Kim, G. S. Diskin, J. P. Digangi, Y. Choi, S. E. Pusede, P. O. Wennberg, M. J. Kim, J. D. Crounse, A. P. Teng, R. C. Cohen, P. S. Romer, W. Brune, A. Wisthaler, T. Mikoviny, J. L. Jimenez, P. Campuzano-Jost, B. A. Nault, A. Weinheimer, S. R. Hall and K. Ullmann, An investigation of petrochemical emissions during KORUS-AQ: Ozone production, reactive nitrogen evolution, and aerosol production, *Elem. Sci. Anth.*, 2022, **10**, 00079.

12 E. Aruffo, F. Biancofiore, P. Di Carlo, M. Busilacchio, M. Verdecchia, B. Tomassetti, C. Dari-Salisburgo, F. Giammaria, S. Bauguitte, J. Lee, S. Moller, J. Hopkins, S. Punjabi, S. J. Andrews, A. C. Lewis, P. I. Palmer, E. Hyer, M. Le Breton and C. Percival, Impact of biomass burning emission on total peroxy nitrates: fire plume identification during the BORTAS campaign, *Atmos. Meas. Tech.*, 2016, **9**, 5591–5606.

13 M. M. Roy, HPLC analysis of aldehydes in automobile exhaust gas: Comparison of exhaust odor and irritation in different types of gasoline and diesel engines, *Energy Convers. Manage.*, 2008, **49**, 1111–1118.

14 H. B. Singh and P. L. Hanst, Peroxyacetyl nitrate (PAN) in the unpolluted atmosphere – an important reservoir for nitrogen oxides, *Geophys. Res. Lett.*, 1981, **8**, 941–944.

15 E. V. Fischer, D. J. Jacob, R. M. Yantosca, M. P. Sulprizio, D. B. Millet, J. Mao, F. Paulot, H. B. Singh, A. Roiger, L. Ries, R. W. Talbot, K. Dzepina and S. Pandey Deolal, Atmospheric peroxyacetyl nitrate (PAN): a global budget and source attribution, *Atmos. Chem. Phys.*, 2014, **14**, 2679–2698.

16 O. C. Taylor, Importance of Peroxyacetyl Nitrate (PAN) as a Phytotoxic Air Pollutant, *J. Air Pollut. Control Assoc.*, 1969, **19**, 347–351.

17 A. P. Altshuller, Assessment of the Contribution of Chemical Species to The Eye Irritation Potential of Photochemical Smog, *J. Air Pollut. Control Assoc.*, 1978, **28**, 594–598.

18 R. M. LoPachin and T. Gavin, Molecular Mechanisms of Aldehyde Toxicity: A Chemical Perspective, *Chem. Res. Toxicol.*, 2014, **27**, 1081–1091.

19 R. K. Talukdar, J. B. Burkholder, A. M. Schmoltner, J. M. Roberts, R. R. Wilson and A. R. Ravishankara, Investigation of the loss processess for peroxyacetyl nitrate in the atmosphere – UV Photolysis and reaction with OH, *J. Geophys. Res.*, 1995, **100**, 14163–14173.

20 W. Schrimpf, K. Lienaerts, K. P. Muller, J. Rudolph, R. Neubert, W. Schussler and I. Levin, Dry deposition of peroxyacetyl nitrate (PAN): Determination of its deposition velocity at night from measurements of the atmospheric PAN and ^{222}Radon concentration gradient, *Geophys. Res. Lett.*, 1996, **23**, 3599–3602.

21 A. A. Turnipseed, L. G. Huey, E. Nemitz, R. Stickel, J. Higgs, D. J. Tanner, D. L. Slusher, J. P. Sparks, F. Flocke and A. Guenther, Eddy covariance fluxes of peroxyacetyl nitrates (PANs) and NO_y to a coniferous forest, *J. Geophys. Res.*, 2006, **111**, D09304.

22 G. M. Wolfe, J. A. Thornton, R. L. N. Yatavelli, M. McKay, A. H. Goldstein, B. LaFranchi, K. E. Min and R. C. Cohen, Eddy covariance fluxes of acyl peroxy nitrates (PAN, PPN and MPAN) above a Ponderosa pine forest, *Atmos. Chem. Phys.*, 2009, **9**, 615–634.

23 C. T. Pate, R. Atkinson and J. N. Pitts, Rate constants for the gas phase reaction of peroxyacetyl nitrate with selected atmospheric constituents, *J. Environ. Sci. Health, Part A*, 1976, **11**, 19–31.

24 R. A. Cox and M. J. Roffey, Thermal decomposition of peroxyacetylnitrate in the presence of nitric oxide, *Environ. Sci. Technol.*, 1977, **11**, 900–906.

25 D. G. Hendry and R. A. Kenley, Generation of peroxy radicals from peroxy nitrates (RO_2NO_2). Decomposition of peroxyacyl nitrates, *J. Am. Chem. Soc.*, 1977, **99**, 3198–3199.

26 R. Guicherit, *Photochemical Smogformation in the Netherlands*, TNO, Commissie Milieuprojecten, Nederlandse Organisatie voor Toegepast Natuurwetenschappelijk Onderzoek, 1978.

27 J. M. Roberts and S. B. Bertman, The thermal decomposition of peroxyacetic nitric anhydride (PAN) and peroxymethacrylic nitric anhydride (MPAN), *Int. J. Chem. Kinet.*, 1992, **24**, 297–307.

28 E. C. Tuazon, W. P. L. Carter and R. Atkinson, Thermal decomposition of peroxyacetyl nitrate and reactions of acetyl peroxy radicals with nitric oxide and nitrogen dioxide over the temperature range 283–313 K, *J. Phys. Chem.*, 1991, **95**, 2434–2437.

29 I. Bridier, F. Caralp, H. Loirat, R. Lesclaux, B. Veyret, K. H. Becker, A. Reimer and F. Zabel, Kinetic and Theoretical Studies of the reactions $CH_3C(O)O_2$+NO_2+M <-> $CH_3C(O)O_2NO_2$+M between 248 K and 393 K and between 30 Torr and 760 Torr, *J. Phys. Chem.*, 1991, **95**, 3594–3600.

30 N. Roumelis and S. Glavas, Thermal decomposition of peroxyacetyl nitrate in the presence of O_2, NO_2 and NO, *Monatsh. Chem.*, 1992, **123**, 63–72.
31 D. Grosjean, E. Grosjean and E. L. Williams, Thermal decomposition of PAN, PPN and vinyl-PAN, *J. Air Waste Manage. Assoc.*, 1994, **44**, 391–396.
32 J. Sehested, L. K. Christensen, T. Mogelberg, O. J. Nielsen, T. J. Wallington, A. Guschin, J. J. Orlando and G. S. Tyndall, Absolute and relative rate constants for the reactions $CH_3C(O)O_2$+NO and $CH_3C(O)O_2$+NO_2 and thermal stability of $CH_3C(O)O_2NO_2$, *J. Phys. Chem. A*, 1998, **102**, 1779–1789.
33 M. Kabir, S. Jagiella and F. Zabel, Thermal Stability of n-Acyl Peroxynitrates, *Int. J. Chem. Kinet.*, 2014, **46**, 462–469.
34 G. Mineshos and S. Glavas, Thermal decomposition of peroxypropionyl nitrate: Kinetics of the formation of nitrogenous products, *React. Kinet. Catal. Lett.*, 1991, **45**, 305–312.
35 F. Kirchner, A. Mayer-Figge, F. Zabel and K. H. Becker, Thermal stability of Peroxynitrates, *Int. J. Chem. Kinet.*, 1999, **31**, 127–144.
36 D. Grosjean, E. Grosjean and E. L. Williams, Thermal-Decomposition of C_3-Substituted Peroxyacyl Nitrates, *Res. Chem. Intermed.*, 1994, **20**, 447–461.
37 P. R. Veres and J. M. Roberts, Development of a photochemical source for the production and calibration of acyl peroxynitrate compounds, *Atmos. Meas. Tech.*, 2015, **8**, 2225–2231.
38 A. Furgeson, L. H. Mielke, D. Paul and H. D. Osthoff, A photochemical source of peroxypropionic and peroxyisobutanoic nitric anhydride, *Atmos. Environ.*, 2011, **45**, 5025–5032.
39 N. D. Rider, Y. M. Taha, C. A. Odame-Ankrah, J. A. Huo, T. W. Tokarek, E. Cairns, S. G. Moussa, J. Liggio and H. D. Osthoff, Efficient photochemical generation of peroxycarboxylic nitric anhydrides with ultraviolet light-emitting diodes, *Atmos. Meas. Tech.*, 2015, **8**, 2737–2748.
40 T. W. Tokarek, J. A. Huo, C. A. Odame-Ankrah, D. Hammoud, Y. M. Taha and H. D. Osthoff, A gas chromatograph for quantification of peroxycarboxylic nitric anhydrides calibrated by thermal dissociation cavity ring-down spectroscopy, *Atmos. Meas. Tech.*, 2014, **7**, 3263–3283.
41 L. H. Mielke and H. D. Osthoff, On quantitative measurements of peroxycarboxylic nitric anhydride mixing ratios by thermal dissociation chemical ionization mass spectrometry, *Int. J. Mass Spectrom.*, 2012, **310**, 1–9.
42 K. D. Easterbrook, M. A. Vona, K. Nayebi-Astaneh, A. M. Miller and H. D. Osthoff, Measurement of Henry's law and liquid-phase loss rate constants of peroxypropionic nitric anhydride (PPN) in deionized water and in n-octanol, *Atmos. Chem. Phys.*, 2023, **23**, 311–322.
43 P. W. Villalta and C. J. Howard, Direct kinetics study of the $CH_3C(O)O_2$+NO reaction using chemical ionization mass spectrometry, *J. Phys. Chem.*, 1996, **100**, 13624–13628.
44 A. H. Laufer and A. Fahr, Reactions and Kinetics of Unsaturated C_2 Hydrocarbon Radicals, *Chem. Rev.*, 2004, **104**, 2813–2832.
45 M. Martínez-Ávila, J. Peiró-García, V. c. M. Ramírez-Ramírez and I. Nebot-Gil, Ab initio study on the mechanism of the HCO+O_2→HO_2+CO reaction, *Chem. Phys. Lett.*, 2003, **370**, 313–318.
46 H. B. Singh and L. J. Salas, Methodology for the analysis of Peroxyacetyl nitrate (PAN) in the unpolluted atmosphere, *Atmos. Environ.*, 1983, (17), 1507–1516.
47 D. Paul and H. D. Osthoff, Absolute Measurements of Total Peroxy Nitrate Mixing Ratios by Thermal Dissociation Blue Diode Laser Cavity Ring-Down Spectroscopy, *Anal. Chem.*, 2010, **82**, 6695–6703.
48 I. Livingston, *Calgary smothered in wildfire smoke, as plumes surge into Lower 48 states*, The Washington Post, 2023, retrieved online at **https://www.washingtonpost.com/weather/2023/05/17/calgary-wildfire-smoke-alberta-united-states/**.
49 O. R. Cooper, K.-L. Chang, K. Bates, S. S. Brown, W. S. Chace, M. M. Coggon, A. M. Gorchov Negron, A. M. Middlebrook, J. Peischl, A. Piasecki, N. Schafer, C. E. Stockwell, S. Wang, C. Warneke, K. Zuraski, K. Miyazaki, V. H. Payne, E. A. Pennington, J. R. Worden, K. W. Bowman and B. C. McDonald, Early Season 2023 Wildfires Generated Record-Breaking Surface Ozone Anomalies Across the U.S. Upper Midwest, *Geophys. Res. Lett.*, 2024, **51**, e2024GL111481.
50 T. Joo, M. J. Rogers, C. Soong, T. Hass-Mitchell, S. Heo, M. L. Bell, N. L. Ng and D. R. Gentner, Aged and Obscured Wildfire Smoke Associated with Downwind Health Risks, *Environ. Sci. Technol. Lett.*, 2024, **11**, 1340–1347.
51 S. S. Brown and J. Stutz, Nighttime radical observations and chemistry, *Chem. Soc. Rev.*, 2012, **41**, 6405–6447.
52 X. X. Zhao and F. L. Liu, Mechanism for the Gas-Phase Hydrogen Fluoride-Mediated Decomposition of Peroxyacetyl Nitrate (PAN) Studied by DFT Method, *Int. J. Quantum Chem.*, 2010, **110**, 1214–1223.
53 P. W. Villalta, E. R. Lovejoy and D. R. Hanson, Reaction probability of peroxyacetyl radical on aqueous surfaces, *Geophys. Res. Lett.*, 1996, **23**, 1765–1768.
54 J. F. Doussin, B. Picquet-Varrault, R. Durand-Jolibois, H. Loirat and P. Carlier, A visible and FTIR spectrometric study of the nighttime chemistry of acetaldehyde and PAN under simulated atmospheric conditions, *J. Photochem. Photobiol., A*, 2003, **157**, 283–293.
55 P. B. Shepson, D. R. Hastie, K. W. So and H. I. Schiff, Relationships between PAN, PPN and O_3 at urban and rural sites in Ontario, *Atmos. Environ., Part A*, 1992, **26**, 1259–1270.
56 Z. C. J. Decker, M. A. Robinson, K. C. Barsanti, I. Bourgeois, M. M. Coggon, J. P. DiGangi, G. S. Diskin, F. M. Flocke, A. Franchin, C. D. Fredrickson, G. I. Gkatzelis, S. R. Hall, H. Halliday, C. D. Holmes, L. G. Huey, Y. R. Lee, J. Lindaas, A. M. Middlebrook, D. D. Montzka, R. Moore, J. A. Neuman, J. B. Nowak, B. B. Palm, J. Peischl, F. Piel, P. S. Rickly, A. W. Rollins, T. B. Ryerson, R. H. Schwantes, K. Sekimoto, L. Thornhill, J. A. Thornton, G. S. Tyndall, K. Ullmann, P. Van Rooy, P. R. Veres, C. Warneke, R. A. Washenfelder, A. J. Weinheimer, E. Wiggins,

E. Winstead, A. Wisthaler, C. Womack and S. S. Brown, Nighttime and daytime dark oxidation chemistry in wildfire plumes: an observation and model analysis of FIREX-AQ aircraft data, *Atmos. Chem. Phys.*, 2021, **21**, 16293–16317.

57 M. Sun, Y. Zhou, Y. Wang, X. Qiao, J. Wang and J. Zhang, Heterogeneous Reaction of Peroxyacetyl Nitrate on Real-World $PM_{2.5}$ Aerosols: Kinetics, Influencing Factors, and Atmospheric Implications, *Environ. Sci. Technol.*, 2022, **56**, 9325–9334.

58 M. L. Wesely and B. B. Hicks, A review of the current status of knowledge on dry deposition, *Atmos. Environ.*, 2000, **34**, 2261–2282.